

THE MID-INFRARED ENVIRONMENTS OF HIGH-REDSHIFT RADIO GALAXIES

AUDREY GALAMETZ^{1,2}, DANIEL STERN¹, CARLOS DE BREUCK³, NINA HATCH⁴, JACK MAYO⁵,
GEORGE MILEY⁶, ALESSANDRO RETTURA⁷, NICK SEYMOUR⁸, S. ADAM STANFORD⁹, JOËL VERNET³

Draft version July 20, 2018

ABSTRACT

Taking advantage of the impressive sensitivity of *Spitzer* to detect massive galaxies at high redshift, we study the mid-infrared environments of powerful, high-redshift radio galaxies at $1.2 < z < 3$. Galaxy cluster member candidates were isolated using a single *Spitzer*/IRAC mid-infrared color criterion, $[3.6] - [4.5] > -0.1$ (AB), in the fields of 48 radio galaxies at $1.2 < z < 3$. Using a counts-in-cell analysis, we identify a field as overdense when 15 or more red IRAC sources are found within $1'$ (i.e., 0.5 Mpc at $1.2 < z < 3$) of the radio galaxy to the 5σ flux density limits of our IRAC data ($f_{4.5} = 13.4\mu\text{Jy}$). We find that radio galaxies lie preferentially in medium to dense regions, with 73% of the targeted fields denser than average. Our (shallow) 120s data permit the rediscovery of previously known clusters and protoclusters associated with radio galaxies as well as the discovery of new promising galaxy cluster candidates at $z > 1.2$.

Subject headings: galaxies: active - galaxies: clusters: general - galaxies: high redshift - infrared

1. INTRODUCTION

The classical technique of finding distant galaxy clusters from the extended X-ray emission associated with their intracluster medium is very effective at finding clusters out to $z \sim 1$, but rapidly becomes insensitive for cluster searches beyond $z \sim 1.2$ (for a detailed review of X-ray selected clusters, see Rosati et al. 2002). The challenge of using X-ray observations to find the most distant clusters is primarily due to the $(1+z)^4$ fading of the X-ray surface brightness. While X-ray selection is very effective at finding massive structures at moderate redshifts and large samples are expected from the all-sky eROSITA soft X-ray telescope after it launches in 2013 (Cappelluti et al. 2011), X-ray selection is unlikely to find the most distant clusters and proto-clusters.

Another proven method to identify distant clusters is by searching wide-field imaging surveys for the red sequence of early-type galaxies. Such red sequence searches were initially introduced using solely optical data (e.g., Gladders & Yee 2000), and have identified hundreds of clusters out to $z \sim 1$. More recently, the *Spitzer* Adaptation of the Red-sequence Cluster Survey (SpARCS; Wilson et al. 2009) has pushed this method to redder wavelengths and thus to higher redshifts. SpARCS has identified clusters out to $z \sim 1.3$. However, a weakness of this approach is that it requires the presence of a

well-formed red sequence of early-type galaxies. Such a sequence might not yet exist as we approach the epoch of cluster formation.

Other field studies such as the IRAC Shallow Survey (ISCS; Stanford et al. 2005; Brodwin et al. 2006; Eisenhardt et al. 2008) also used the Infrared Array Camera (IRAC; Fazio et al. 2004) onboard *Spitzer* to expand the sample of galaxy clusters known at $z > 1.2$. In particular, the ISCS identifies clusters on the basis of photometric redshifts and does not require a red sequence. IRAC is an extremely sensitive tool for finding massive galaxies at high redshift since their $4.5\mu\text{m}$ flux densities remain nearly constant at $0.7 < z < 2.5$ due to a negative and favorable k -correction (e.g., Eisenhardt et al. 2008).

Papovich (2008) used a simple IRAC color criterion (see Section 4) to highlight overdensities of high-redshift galaxies in the *Spitzer* Wide-Infrared Extragalactic (SWIRE; Lonsdale et al. 2003) survey and, in doing so, isolated one of the highest redshift clusters known to date, ClG J0218-0510 at $z = 1.62$ in the *XMM-LSS* field of SWIRE. Spectroscopic follow-up confirmed 9 members (Papovich et al. 2010). This same cluster was independently discovered by Tanaka et al. (2010) using photometric redshifts. This second team found two concentrations of galaxies at $z_{\text{ph}} \sim 1.6$, one of them associated with extended X-ray emission. They spectroscopically confirmed six members.

These various IRAC surveys have the strong advantage of providing uniformly selected galaxy cluster samples over wide areas. Such uniform cluster samples are beneficial for a range of studies, including probing the formation epoch of the early-type galaxy populations (e.g., Mancone et al. 2010; Rettura et al. 2011) and statistical probes of cosmological parameters (e.g., Vikhlinin et al. 2009; Stern et al. 2010).

However, clusters are rare objects and finding larger samples of massive high-redshift galaxy clusters would require field surveys even wider than the several tens of square-degrees which is the current state-of-the-art. Work has been done using targeted cluster searches, i.e., focusing on regions of the sky suspected to host

¹ Jet Propulsion Laboratory, California Institute of Technology, 4800 Oak Grove Dr., Pasadena, CA 91109, USA

² INAF - Osservatorio di Roma, Via Frascati 33, I-00040, Monteporzio, Italy [e-mail: audrey.galametz@oa-roma.inaf.it]

³ European Southern Observatory, Karl-Schwarzschild-Strasse 2, D-85748 Garching, Germany

⁴ University of Nottingham, School of Physics and Astronomy, Nottingham NG7 2RD

⁵ Institute for Astronomy, Royal Observatory, Blackford Hill, Edinburgh, EH9 3HJ, UK

⁶ Leiden Observatory, University of Leiden, P.B. 9513, Leiden 2300 RA, The Netherlands

⁷ Department of Physics and Astronomy, University of California, Riverside, CA 92521, USA

⁸ Mullard Space Science Laboratory, UCL, Holmbury St Mary, Dorking, Surrey, RH5 6NT

⁹ Institute of Geophysics and Planetary Physics, Lawrence Livermore National Laboratory, Livermore, CA 94550

overdensities of galaxies. For example, powerful, high-redshift radio galaxies¹ (HzRGs hereafter) are among the most massive galaxies known up to very high redshift (Seymour et al. 2007) and, as such, are suspected to lie preferentially in overdense regions. Studies of HzRG environments have revealed excesses of extremely red objects (EROs; Stern et al. 2003; Best et al. 2003), line emitters detected through narrow-band imaging (Pentericci et al. 2000; Venemans et al. 2007, and references therein) and submillimetre galaxies (Stevens et al. 2003; De Breuck et al. 2004; Greve et al. 2007) in the fields of HzRGs out to $z \sim 5$. A range of complementary studies have made use of optical through mid-infrared observations to isolate candidate cluster members associated with radio galaxies (Kodama et al. 2007; Galametz et al. 2009, 2010a; Hatch et al. 2010; Mayo et al. 2012 in press).

Recently, Falder et al. (2010) extended this cluster selection technique to a large sample of high-redshift active galactic nuclei (AGN) at $z \sim 1$. Their sample, observed at $3.6\mu\text{m}$ with IRAC, included both radio-loud and radio-quiet AGN. They found excesses of $3.6\mu\text{m}$ sources within 300 kpc of the AGN, as well as evidence for a positive correlation between source density and radio power.

In this paper, we use mid-infrared 3.6 and $4.5\mu\text{m}$ observations of radio galaxies at $1.2 < z < 3$ to study their environments and identify their possible association with high-redshift galaxy clusters. Note that we use the designation ‘cluster’ to refer to both cluster- and protocluster-like structures. The paper is organized as follows. The HzRG sample and catalog extraction are presented in §2 and §3. In §4, we introduce our IRAC selection criterion for high-redshift cluster member candidates. In §5, we present the counts-in-cell analysis used to isolate overdensities associated with HzRGs. We also present the spatial distribution of IRAC-selected sources in our most promising high-redshift cluster candidates in §6. We discuss our $z > 3$ fields in §7 and present our conclusions in §8. Throughout, we assume a Λ CDM cosmology with $H_0 = 70 \text{ km s}^{-1} \text{ Mpc}^{-1}$, $\Omega_m = 0.3$ and $\Omega_\Lambda = 0.7$. Magnitudes and colors are expressed in the AB photometric system unless stated otherwise.

2. RADIO GALAXY SAMPLE AND IRAC DATA

Our primary HzRG sample comes from the *Spitzer* High-Redshift Radio Galaxy survey (SHzRG; Seymour et al. 2007, De Breuck et al. 2010). Most of the sources were observed with IRAC during Cycle 1 (PID 3329; PI Stern) with typical integration times of 120s in all four IRAC bands (see Table 2). Some fields were imaged more deeply using guaranteed time observations (see Table 3). Details on the IRAC reductions can be found in Seymour et al. (2007) and De Breuck et al. (2010). Mayo et al. 2012 (in press) report on the MIPS $24\mu\text{m}$ environments of 64 of these fields.

The initial SHzRG sample was designed to homogeneously cover the $L_{3\text{GHz}}$ radio luminosity - redshift plane. More recent work on the SHzRG sample, including this paper, instead use $L_{500\text{MHz}}$, which is a more isotropic measure of AGN power (De Breuck et al. 2010). This

leads to a slightly less uniform distribution in the $L_{500\text{MHz}}$ radio luminosity - redshift plane (see Fig. 2 of De Breuck et al. 2010). We will keep this in mind by using appropriate statistical tests later in the paper (see Section 5.3).

In 2009, we obtained deeper 1600s IRAC observations of a sample of 10 radio galaxies (see Table 3, PID 60112; PI Hatch) at 3.6 and $4.5\mu\text{m}$. Six of these fields were already part of the initial shallower sample. In this paper, we make use of the deeper data when available. These deeper data were reduced as in Seymour et al. (2007).

The goal of our study is to isolate galaxy clusters at high redshift using only mid-infrared data. As described below, the IRAC criterion applied in this work (see Section 4) is optimal for isolating galaxy structures at $1.2 < z < 3$. We therefore concentrate our analysis on the 48 HzRG fields in this redshift range. We also analyze the 25 HzRG fields at $z < 1.2$ and $3 < z < 5.2$ from our sample in an identical manner and use these fields as a control sample.

3. CATALOG EXTRACTION AND FLUX LIMITS

In order to study the mid-infrared environments of our HzRG sample, we analyzed the available *Spitzer* data using standard techniques.

We restricted the analysis to areas covered for at least 60s in both IRAC channel 1 ($3.6\mu\text{m}$) and 2 ($4.5\mu\text{m}$). The central part ($\sim 1' \times 1'$) exposure time is 120s. We checked the images by eye and flagged zones affected by artifacts (e.g., scattered light). Source extraction was done using SExtractor (Bertin & Arnouts 1996) in dual image mode, using the $4.5\mu\text{m}$ frame as the detection image. We used SExtractor parameters from Lacy et al. (2005) which have been optimized for analysis of IRAC data, and measured photometry in $3''$ diameter apertures. These magnitudes were then corrected to total magnitudes using corrections determined by the IRAC instrument team (M. Lacy, private communication). Specifically, the aperture corrections applied were 1.68 and 1.81 for channels 1 and 2 respectively.

Limiting flux densities for each image were determined from randomly placed $3''$ diameter apertures. For the SHzRG fields, the limiting flux densities were determined on the area covered by 120s exposure which extends beyond a radius of $1'$ from the HzRG i.e., the size of the cell on which this work is conducted. To allow for uniform analysis of our large data set, we adopt a conservative flux density cut corresponding to the 5σ depth of our shallowest data, i.e., $f_{3.6} = 11.0\mu\text{Jy}$ ($[3.6] = 21.3$) and $f_{4.5} = 13.4\mu\text{Jy}$ ($[4.5] = 21.1$)².

Recently, Mancone et al. (2010) derived the 3.6 and $4.5\mu\text{m}$ luminosity functions of galaxy clusters out to $z \sim 1.5$. They found $[3.6]^* \sim 20.0$ and $[4.5]^* \sim 20.1$ for clusters at $z \sim 1.2$. Similarly, Strazzullo et al. (2006) derived the K_s -band luminosity function of clusters at $z \sim 1.2$. Using the Bruzual & Charlot (2003) model of a 2 Gyr-old single burst galaxy with an exponentially declining star formation history with $\tau = 0.1$, we find that $K - [3.6] \sim 0.3$ at $z \sim 1.2$ with a nearly constant $K - [3.6]$ color at $1 < z < 2$. Strazzullo et al. (2006) find that $K_s^* \sim 20.5$ at $z \sim 1.2$, corresponding to $[3.6]^* \sim 20.2$, in

¹ Following Seymour et al. (2007), we define a HzRG as a radio galaxy above a redshift of one with a *restframe* 3 GHz luminosity greater than $10^{26} \text{ W Hz}^{-1}$.

² Magnitudes in IRAC channels 1 and 2 are indicated by $[3.6]$ and $[4.5]$, respectively, and $m_{\text{AB}} = 23.9 - 2.5 \log(f_\nu/1\mu\text{Jy})$.

agreement with the work of Mancone et al. (2010). To our adopted limiting magnitude of $[3.6] = 21.3$, our shallow 120s observations are therefore sensitive to galaxies one magnitude fainter than L^* at $z \sim 1.2$. As shown in Mancone et al. (2010), m^* should remain relatively constant out to $z \sim 2$ assuming cluster galaxies form at $z \geq 2.5$.

4. COLOR SELECTION OF CLUSTER MEMBER CANDIDATES

One of the main spectral features in the spectral energy distributions (SEDs) of galaxies is the $1.6\mu\text{m}$ bump, caused by a minimum in the opacity of the H^- ion which is present in the atmospheres of cool stars (John 1988). This bump, seen in the SEDs of all normal galaxies, has often been used as an efficient photometric redshift indicator (e.g., Simpson & Eisenhardt 1999; Sorba & Sawicki 2010, and references therein). Fig. 1 shows the position of the $1.6\mu\text{m}$ bump for galaxies at $z = 1$ and $z = 2$ relative to the IRAC 3.6 and $4.5\mu\text{m}$ bands. The bump enters the IRAC bands at $z \sim 1$ and shifts beyond $3.6\mu\text{m}$ at $z \sim 1.2$. This causes lower redshift galaxies to have blue $[3.6] - [4.5]$ colors, while galaxies above $z \sim 1.2$ become red across these passbands.

Combining a wide variety of composite stellar population models and spectroscopy of high-redshift galaxies in the GOODS-S and AEGIS DEEP2 fields, Papovich (2008) confirmed that $[3.6] - [4.5] > -0.1$ (i.e., $f_{3.6}/f_{4.5} < 1.1$) is very efficient at isolating $z > 1.2$ galaxies. They showed that only a minority population of $0.2 < z < 0.5$ strongly star-forming galaxies with a strong warm dust contribution have such red colors and that about 80% of galaxies with $[3.6] - [4.5] > -0.1$ are at $z > 1$. Specifically, based on redshifts from the DEEP2 redshift survey, Papovich (2008) show that $\sim 50\%$ of galaxies at $z > 1.1$ have red IRAC colors, with this percentage increasing to $\sim 75\%$ for $z > 1.2$ galaxies and reaching $\sim 90\%$ for $z > 1.3$ galaxies. In the later analysis we use this color cut to study the fields of HzRGs at $z > 1.2$, though we caution the reader that the efficiency of the selection criterion is diminished in the $1.2 < z < 1.3$ range. At any rate, only one HzRG from our sample, 3C266 at $z = 1.275$, is in this redshift range. Finally, we note that, contrary to other high-redshift galaxy selection techniques such as the BzK selection for $z > 1.4$ galaxies (Daddi et al. 2000) or the near-infrared selection techniques for $z > 1.6$ galaxies (Kajisawa et al. 2006; Galametz et al. 2010b), this single IRAC color criterion does not permit the segregation between galaxy types since it is based on a spectro-photometric property of essentially all galaxy populations (Papovich 2008).

This red IRAC color criterion will identify a few additional astronomical populations, but none are expected to be significant contaminations. Most stars have $[3.6] - [4.5] \sim -0.5$ (i.e., Vega color of zero). Stern et al. (2007) shows that only brown dwarfs cooler than spectral type T3 have such red colors ($[3.6] - [4.5] > -0.07$) and such objects will be rare in a flux-limited survey at our depth. Extremely dusty stars, such as asymptotic giant branch (AGB) stars, will also have red IRAC colors (e.g., Eisenhardt et al. 2010). However, they are likewise expected to be quite rare in a flux-limited survey primarily targeted at high Galactic latitudes.

At all redshifts, most powerful AGN ($> 95\%$) have

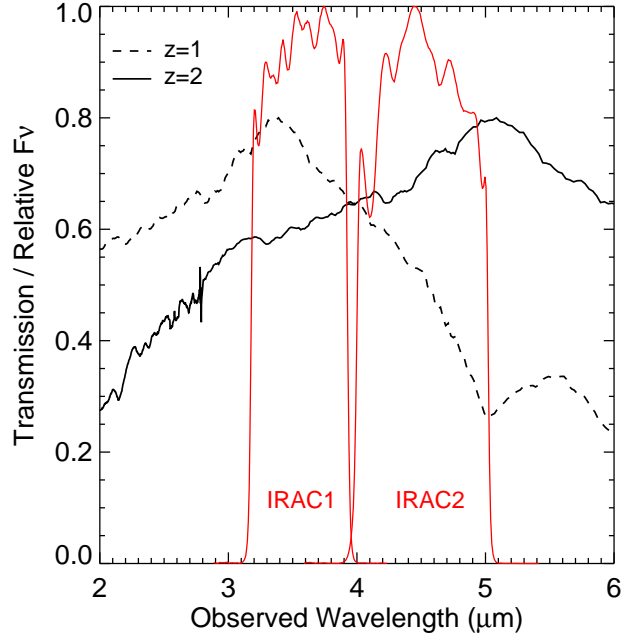


FIG. 1.— Spectral energy distribution of a 2 Gyr-old galaxy redshifted to $z = 1$ (dashed line) and $z = 2$ (solid line) assuming a rapid ($\tau = 0.1$ Gyr) exponentially declining star-formation history. The strongest feature in this wavelength range is the restframe $1.6\mu\text{m}$ stellar bump. Transmission curves for IRAC channel 1 and 2 are overplotted for reference.

$[3.6] - [4.5] > -0.1$ and will be selected by this IRAC criterion. Stern et al. (2005) measure a surface density of 275 AGN per deg^2 in the Boötes field down to flux density limits of $f_{3.6} = 12.3\mu\text{Jy}$ and $f_{4.5} = 15.4\mu\text{Jy}$. Using IRAC catalogues available for the Boötes field (see Section 5.2 for details), we derive a density of $\sim 28,700$ red IRAC-selected sources per deg^2 to the same depth. We therefore expect contamination by AGN to represent less than 1% of sources with $[3.6] - [4.5] > -0.1$ at the depth of our survey.

According to models for passively evolving stellar populations formed at high-redshift, negative k -corrections provide a nearly constant $4.5\mu\text{m}$ flux density at $z > 0.7$ and up to high redshifts. Fig. 2 shows the evolution of the $4.5\mu\text{m}$ flux density and the $[3.6] - [4.5]$ color as a function of redshift for various formation redshifts. We make use of the publicly available model calculator EZ Gal³. We use the Maraston (2005) and the Charlot & Bruzual 2007 — an update of Bruzual & Charlot (2003) — models for single stellar populations assuming solar metallicity and a Salpeter initial mass function. The $4.5\mu\text{m}$ flux density is normalized to match the observed $m_{4.5}^*$ of galaxy clusters at $z \sim 0.7$, $[4.5]_{\text{Vega}} = 16.75$. Mancone et al. (2010) studied a large sample of clusters up to $z \sim 1.5$ to derive the $4.5\mu\text{m}$ luminosity function and found that the luminosity function is consistent with a formation redshift $z_f \sim 2 - 3$. Fig. 2 shows that for $z_f = 3$, the $4.5\mu\text{m}$ flux density is relatively constant at $z > 1$. It even decreases (brightens) with redshift as one approaches the galaxy formation epoch.

Mancone et al. (2010) models could not simultane-

³ www.mancone.net/ezgal/model

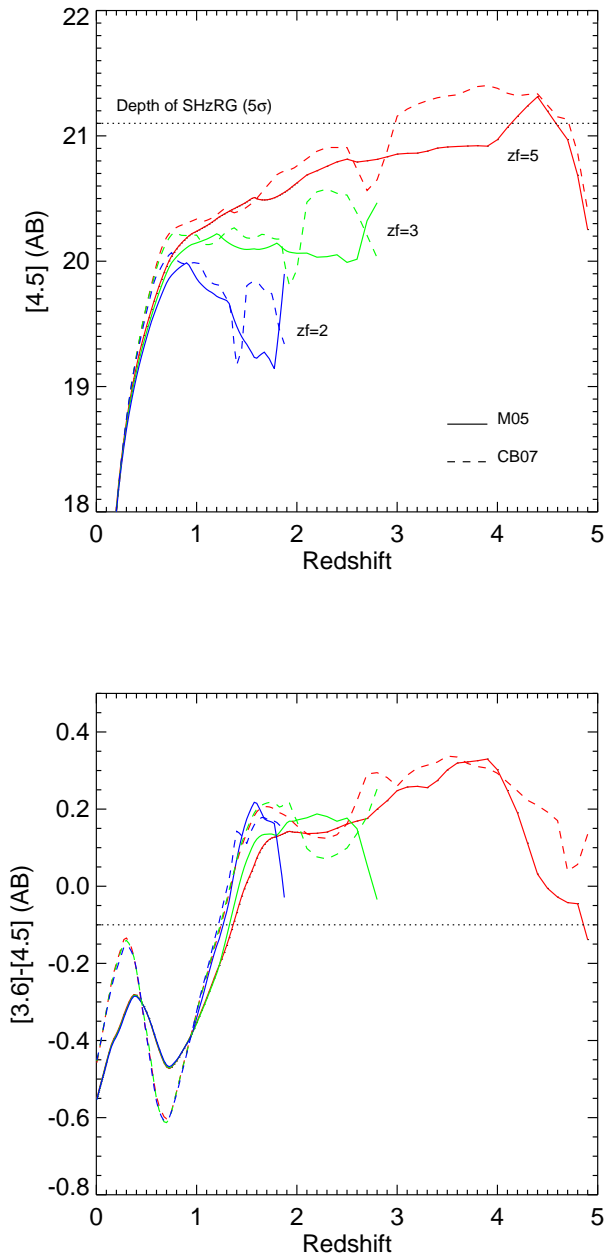


FIG. 2.— Evolution of $4.5\mu\text{m}$ flux density (top panel) and $[3.6] - [4.5]$ color (bottom) versus redshift for single stellar populations with a range of formation redshift, $z_f = 2$ (blue), 3 (green) and 5 (red). Rapid ($\tau = 0.1$ Gyr) exponentially declining star-formation history models, from Maraston et al. 2005 (M05; solid line) and Charlot & Bruzual 2007 (CB07; dashed), were generated with EZ Gal (assuming $[4.5]_{\text{Vega}} = 16.75$ at $z \sim 0.7$; see text for details). At $z > 1$, $[4.5]$ is relatively independent of redshift out to the formation epoch. The dotted lines indicate the $[4.5]$ depth (top) and the $[3.6] - [4.5] > -0.1$ color criterion (bottom) adopted in this work.

ously match the low and high-redshift data; they found that m^* becomes fainter at the highest redshifts probed, interpreted as a possible evidence for galaxy assembly at $z \geq 1.5$. Note, however, that the Mancone et al. (2010) uncertainties increase with redshift, with few of the highest redshift clusters spectroscopically confirmed, and larger systematic uncertainties in subtracting the foreground/background galaxy populations. Numerous authors have investigated the epoch of early-type galaxy assembly, and the results span a wide range of formation redshifts (e.g., van Dokkum 2008; Eisenhardt et al. 2010). A larger sample of high-redshift galaxy clusters is clearly needed to further investigate this question.

In the following, we assume a uniform $[3.6] - [4.5] > -0.1$ color criterion to select high-redshift candidates in the fields of 48 radio galaxies at $1.2 < z < 3$. We consider sources detected to the 5σ depth of our SHzRG sample ($[4.5] = 21.1$). We include sources with $[3.6] - [4.5] > -0.1$ with a $3.6\mu\text{m}$ magnitude fainter than the limits of our SHzRG survey. For such sources, we uniformly assign a lower limit of $[3.6] = 21.3$. Sources selected by these criteria are referred to as ‘red IRAC-selected sources’ or simply as ‘IRAC-selected sources’ in the rest of the paper.

As seen in Fig. 2, our selection criteria should robustly identify clusters across this whole redshift range, assuming cluster galaxy formation and assembly is at similar or higher redshift. The aim of the current work is to test this hypothesis. Current literature only studies evolved populations in clusters out to $z \sim 1.3$, with less certain results for cluster candidates at higher redshifts. Extensive literature from multiple observing programs infer the cluster formation epoch is at higher redshift, with results ranging over the $2 \lesssim z_f \lesssim 5$ range. Given the current state of knowledge, the high redshift end of our analysis is somewhat arbitrary; we could have been more conservative and chosen a lower redshift cut-off, or, in principle, we could have considered a higher redshift cut-off. If we do not find rich fields around our highest redshift HzRGs, multiple explanations are possible. It could mean that clusters do not exist at those redshifts, it could be due to small number statistics, or it could imply issues with the simple evolutionary model we are testing in Fig. 2, a model that is remarkably effective at describing cluster data at $z < 1.3$. In particular, galaxy mergers might cause an evolution of m^* with redshift such that we become less sensitive to clusters at the high-redshift end of our sample. Such a result would be of interest.

5. COUNTS-IN-CELL ANALYSIS

5.1. Counts-in-cell in SWIRE

We use a counts-in-cell analysis to identify overdensities of IRAC red galaxies associated with HzRGs. As a reference field, we analyze the SWIRE (SWIRE; Lonsdale et al. 2003) survey. With its typical 120s exposure, the SWIRE survey reaches slightly deeper than our HzRG data, primarily because it exclusively targets low-background regions of the sky. SWIRE covers $\sim 50 \text{ deg}^2$, split into six independent fields which mitigates the effects of cosmic variance.

To ensure consistency with our analysis of the radio galaxy fields, we build our own catalogues for all six SWIRE fields. As described in Section 3, we use the $4.5\mu\text{m}$ image for source detection and derive photometry

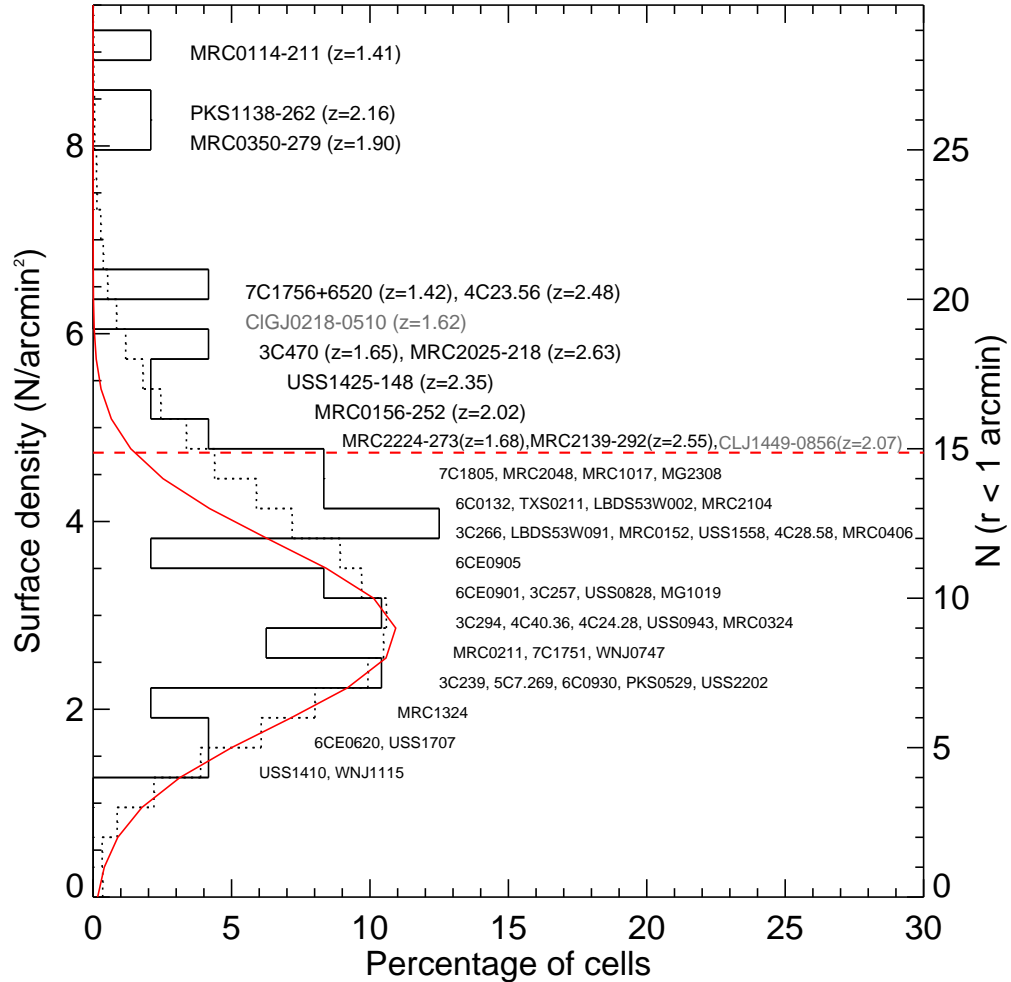


FIG. 3.— Distribution of the surface density of $[3.6] - [4.5] > -0.1$ sources in 20,000 cells of $1'$ radius randomly generated in the six SWIRE fields to the flux density limits of our sample (dotted histogram). The corresponding number of sources per cell is indicated on the right axis. A Gaussian fit of the lower part of the distribution is shown by the red curve and the 2σ deviation above the mean of this distribution by the horizontal dotted line. Each radio galaxy is placed at the vertical axis location corresponding to the surface density of IRAC-selected sources found within $1'$ from the radio galaxy. The solid histogram shows the percentage of radio galaxy fields for a given density. Two examples of known high-redshift galaxy clusters (CLG J0218-0510 and Cl J1449+0856) are also indicated by the gray labels (see §5.2).

from $3''$ diameter apertures, corrected to total magnitudes following Lacy et al. (2005).

At the depth of our survey, we detect the bright end of the galaxy luminosity function, which preferentially populates cluster cores. We therefore adopt a cell size of $1'$ radius, corresponding to ~ 0.5 Mpc at $1 < z < 3$. This distance matches typical cluster r_{200} sizes for $z > 1.3$ mid-infrared selected galaxy clusters (e.g., Wilson et al. 2009).

We generate 20,000 independent (i.e., non-overlapping) circular cells of $1'$ radius, randomly distributed over the six SWIRE fields. Fig. 3 shows the histogram of the surface density of red IRAC-selected sources per cell. The horizontal axis shows the percentage of cells corresponding to a specific surface density. The shape of the distribution is a Gaussian strongly skewed towards higher density cells. We fit the lower half of the distribution (i.e., the distribution of the lower

density regions) by a Gaussian (iteratively clipping at 2σ). The best fit values give a Gaussian centered at $\langle N \rangle = 2.80$ galaxies per arcmin 2 (~ 8.8 sources per cell) with $\sigma_N = 0.97$. We define an overdensity of IRAC-selected sources when a cell is denser than $N + 2\sigma_N \sim 4.74$ galaxies per arcmin 2 — i.e., when at least 15 sources are found within a cell of $1'$ radius. This criterion, for which visual inspection typically registers interesting spatial segregation, is matched by only 9% of the cells in SWIRE.

5.2. Tests on known $z > 1$ galaxy clusters

Before applying our newly defined criterion, we test its efficiency on published clusters at $z > 1$ observed with IRAC. We first study two of the highest redshift clusters known to date: CLG J0218-0510 at $z = 1.62$ (Papovich et al. 2010; Tanaka et al. 2010) and Cl J1449+0856 at $z = 2.07$ (Gobat et al. 2011).

CIG J0218-0510 is located in the XMM field of SWIRE. We select sources with $[3.6] - [4.5] > -0.1$ in the field of CIG J0218-0510 using the catalogues we derived from the SWIRE data (see Section 5). Cl J1449+0856 was discovered in the CNOC 1447+09 field (Yee et al. 2000) and was also first identified as an overdensity of red IRAC-selected galaxies. To date, 11 cluster members have been spectroscopically confirmed (Gobat et al. 2011). We retrieved the IRAC 3.6 and $4.5\mu\text{m}$ reduced post-BCD images of the CNOC 1447+09 field from the *Spitzer* archive (P.I. Fazio) and derived our own catalogue in an identical manner as for the HzRG targets.

For both cluster fields, we select sources with $[3.6] - [4.5] > -0.1$. Fig. 4 shows the spatial distribution of these red sources in the $6' \times 6'$ field around CIG J0218-0510 (top) and Cl J1449+0856 (bottom panel). Large red symbols account for sources detected within the limits applied to our SHzRG sample and smaller gray dots account for sources within the 5σ limits of SWIRE ($f_{3.6} = 3.7\mu\text{Jy}$ and $f_{4.5} = 5.4\mu\text{Jy}$) and CNOC 1447+09 ($f_{3.6} = 2.3\mu\text{Jy}$ and $f_{4.5} = 3.8\mu\text{Jy}$). We also show the spectroscopically confirmed cluster members (black squares) for CIG J0218-0510 (Papovich et al. 2010; Tanaka et al. 2010) and Cl J1449+0856 (R. Gobat, private communication). All of the confirmed members detected at 3.6 and $4.5\mu\text{m}$ have $[3.6] - [4.5] < -0.1$ though some are below the 5σ limits plotted in Fig. 4.

Nineteen red IRAC-selected galaxies are found within $1'$ of the assigned center of CIG J0218-0510 and 15 for Cl J1449+0856. Both clusters are clearly seen as compact concentrations of red galaxies and are selected as overdense fields by our IRAC criteria (see also Fig. 3, gray labels).

An overdensity of EROs was also recently detected in the field of the quasar 3C270.1 at $z = 1.53$ (Haas et al. 2009) suggesting that the quasar is associated with a high-redshift galaxy structure. We retrieved the IRAC post-BCD 3.6 and $4.5\mu\text{m}$ images of this field from the *Spitzer* archive and extracted the corresponding $4.5\mu\text{m}$ selected catalogue. Twenty-four red IRAC-selected sources are found within $1'$ of the quasar. This strengthens past results that the quasar is part of a high-redshift cluster.

Recently, Eisenhardt et al. (2008) identified a large sample of 335 mid-infrared selected galaxy clusters in the Boötes field, including five clusters spectroscopically confirmed at $1.2 < z < 1.5$. The Boötes field was covered by the *Spitzer* Deep, Wide-Field Survey (SDWFS; Ashby et al. 2009), an IRAC survey of 8.5 deg^2 with 5σ depths of 22.9 and 22.4 in 3.6 and $4.5\mu\text{m}$, respectively. We make use of the publicly available $4.5\mu\text{m}$ -selected catalogue of the SDWFS Data Release 1 to derive the number of IRAC-selected sources within $1'$ of the cluster centers. All five $z > 1.2$ confirmed galaxy clusters have 15 or more IRAC-selected sources in the studied cell and would be selected as overdense fields by our IRAC criteria. Of the 40 spectroscopically confirmed members of these clusters at $z > 1.2$ detected at $4.5\mu\text{m}$ (Stanford et al. 2005, Brodwin et al. 2006, Eisenhardt et al. 2008), 25 (63%) have $[3.6] - [4.5] > -0.1$. Considering only cluster members at $z > 1.3$, all 21 galaxies have colors consistent with the red IRAC criterion within the photometric errors. Considering the $z < 1.2$ clusters reported

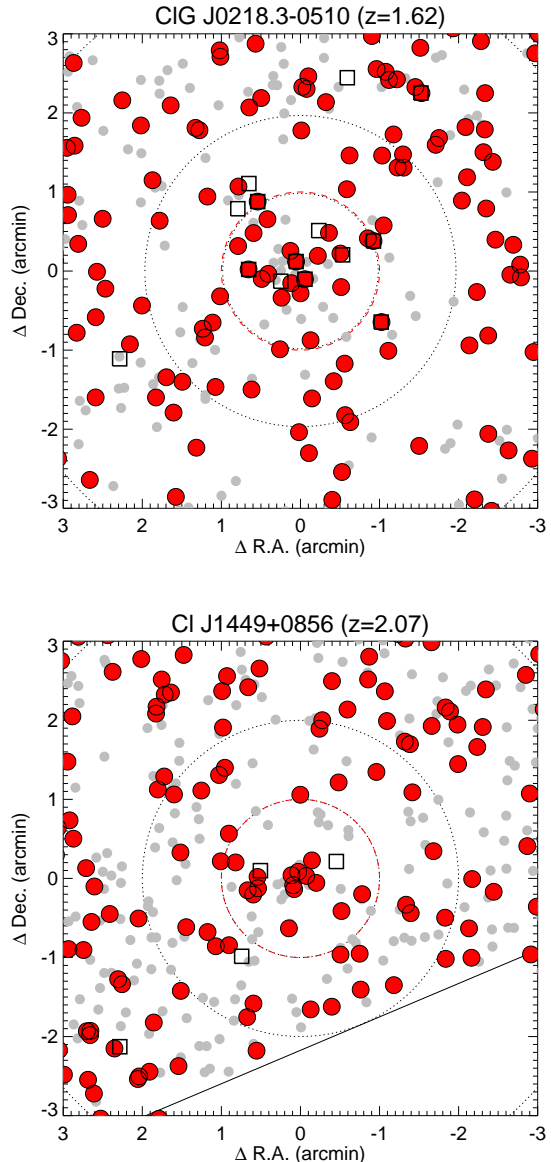


FIG. 4.— Spatial distribution of sources with $[3.6] - [4.5] > -0.1$ in the fields of two spectroscopically confirmed galaxy clusters: CIG J0218.3-0510 ($z = 1.62$; top) and Cl J1449+0856 ($z = 2.07$; bottom); the solid line marks the limit of the area covered by *Spitzer*. Small gray circles indicate sources down to the 5σ depth of the original IRAC data while larger red symbols indicate sources detected to the flux limits of our SHzRG data. Dotted circles illustrate 0.5, 1 and 2 Mpc radii at $z = 1.62$ and $z = 2.07$. A $1'$ radius cell ($\sim 0.5\text{Mpc}$) centered on the adopted cluster center is shown by the red dashed circle. Spectroscopically confirmed members are indicated by black squares. North is up; East is to the left.

in Eisenhardt et al. (2008), only the cluster at $z = 1.161$ would be selected as an overdense field by our red IRAC selection criterion. These results confirm that our IRAC criterion begins to become effective at identifying galaxy clusters at $z > 1.2$ and is quite robust at identifying rich structures at $z > 1.3$.

A large number of high-redshift galaxy cluster candidates were also recently found in SWIRE by the SpARCS survey. We further test our selection criterion on spectroscopically confirmed SpARCS clusters and recover their

two highest redshift galaxy clusters (to date): SpARCS J003550-431224 ($z = 1.34$; Wilson et al. 2009) — a very dense structure with 35 IRAC-selected sources found within $1'$ of the assigned cluster center — and SpARCS J161037+552417 ($z = 1.21$; Demarco et al. 2010) with 19 red IRAC-selected sources. We note that the two $z < 1.2$ clusters published in Demarco et al. 2010 (at $z = 0.871$ and $z = 1.161$) were not recovered.

5.3. Radio galaxy fields

We now determine the number of red IRAC-selected sources within $1'$ of each radio galaxy. Each field is shown in Fig. 3 at the position corresponding to the number of IRAC-selected sources found within $1'$ of the radio galaxies. The density for each field is also reported in Tables 2 and 3 (last column). The solid histogram shows the percentage of radio galaxy fields corresponding to a given density. We find that radio galaxies preferentially lie in medium to dense regions, with 73% ($\pm 12\%$) of the targeted fields denser than the mean of the Gaussian fit to the SWIRE fields. Eleven fields i.e. 23% ($\pm 7\%$) are found with more than 15 red IRAC-selected sources within $1'$ of the central radio galaxy. We conduct a two-sided Kolmogorov-Smirnov statistic between the distributions of densities of IRAC-selected sources in SWIRE and in the HzRG cells and find a probability of only 1.3% that the two distributions are drawn from the same distribution.

From the 20,000 cells we produced in SWIRE, we generated 100,000 random samples of 48 cells and derived the fraction of these sub-samples that have at least 11 2σ -overdense cells. We find that only 0.3% of the sub-samples have a fraction of overdense cells comparable to our radio galaxy sample, confirming that radio galaxies lie preferentially in dense regions.

We discuss our 11 overdense fields in more detail in Section 6. At our bright magnitude limits, we expect to isolate high-redshift galaxy structures that contain many bright ($M^* + 1$ or brighter) galaxies in their cores. We do not rule out the possibility that the other radio galaxies may be associated with less massive and/or less compact galaxy structures.

The sample of radio galaxies covers a wide range of redshift as well as a wide range of radio luminosity. We next consider a possible dependence of overdensity with these two parameters. Fig. 5 and Fig. 6 show the counts-in-cell around the radio galaxies versus redshift and radio luminosity, respectively. We adopt Poissonian errors for the counts-in-cell and use the Gehrels (1986) small number approximation for Poisson distribution. The inset on top of each figure shows the percentage of overdense fields compared to the total number of fields per bin of redshift or radio luminosity.

No significant correlation is observed between overdensity and redshift (Fig. 5). As far as a correlation with radio power is concerned (Fig. 6), we note that 35% ($\pm 13\%$) of radio galaxies with $L_{500\text{MHz}} > 10^{28.6} \text{ W Hz}^{-1}$ are found in overdense fields, compared to 23% of the full sample. This could indicate a positive correlation between overdensity and radio power, a result suggested by past studies (Miley & De Breuck 2008; Falder et al. 2010). However, the Spearman rank correlation coefficient between overdensity and radio power is as low as 0.071. As mentioned in Section 2, there may be a small

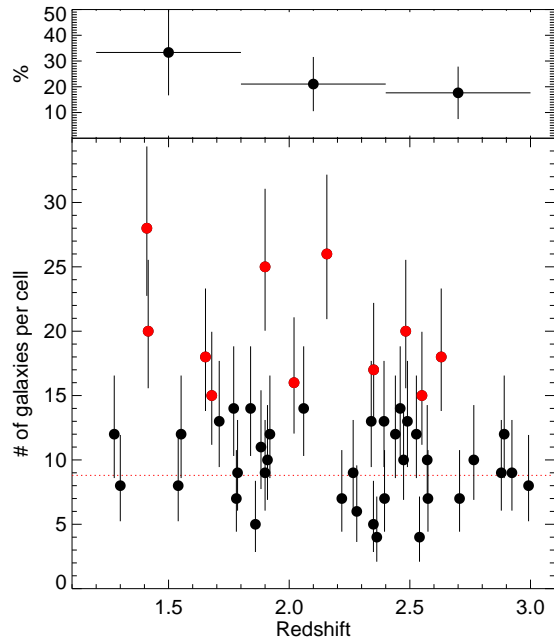


FIG. 5.— Number of $[3.6] - [4.5] > -0.1$ sources within $1'$ of the radio galaxies (and within the 5σ $4.5\mu\text{m}$ limit of our sample) as a function of redshift. Overdense environments are marked in red. The horizontal red line shows the median value (8.8) for a $1'$ radius cell in SWIRE. The top panel shows the percentage of overdense fields relative to the total number of fields per bin of redshift.

degeneracy between $L_{500\text{MHz}}$ and redshift in our sample. A study of the Spearman partial rank correlation coefficient — which takes the correlation of two variables with a third related variable (Macklin 1982) — still do not show any significant correlation between overdensity and radio luminosity. This result is consistent with the absence of correlation observed between overdensity and the density of $24\mu\text{m}$ MIPS-selected sources in the same HzRG sample (Mayo et al. 2012 in press). We conclude that a larger sample, reaching radio luminosities of several orders of magnitude lower, is required to study (and quantify) a possible correlation.

5.4. Analysis of HzRG fields with deeper IRAC data

We also examine fields with at least 1600s IRAC exposures. We adopt correspondingly deeper cuts for the deeper sample ($f_{4.5} = 3.4\mu\text{Jy}$; $[4.5] = 22.6$). Similar to the shallower analysis, we select sources using the criterion $[3.6] - [4.5] > -0.1$. For sources below the deeper $3.6\mu\text{m}$ flux density limits, we uniformly assign a lower limit $[3.6] = 23.0$. The adopted depth corresponds to $\sim M^* + 3$. We derive densities of red IRAC-selected sources within $1'$ of the radio galaxies to these deeper flux limits (Table 1). We find results consistent with our analysis at shallower cuts, recovering PKS1138-262 ($z = 2.156$), MRC0156-252 ($z = 2.016$) and MRC0350-279 ($z = 1.900$) as the densest fields; compared to the average surface density of red IRAC-selected sources in the other radio galaxy fields, the environments of these three radio galaxies are at least 1.5 times richer.

6. CONFIRMED CLUSTERS AND NEW CLUSTER CANDIDATES

Eleven radio galaxy fields present significant overdensities of red sources. Fig. 7 shows the spatial distribution

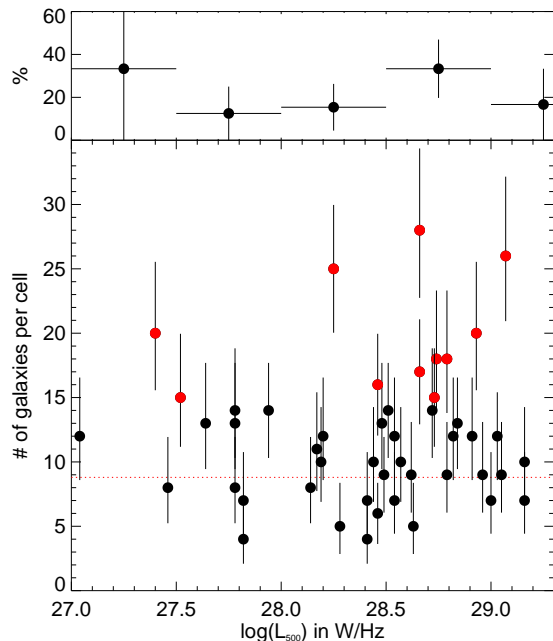


FIG. 6.— Number of $[3.6] - [4.5] > -0.1$ sources within $1'$ of the radio galaxies as a function of radio luminosity. Symbols are as in Fig. 5. We note that the majority of our cluster candidates are found around HzRGs with $L_{500\text{MHz}} > 10^{28.6} \text{ W Hz}^{-1}$ suggesting that more powerful radio galaxies reside in denser environments.

TABLE 1
SURFACE DENSITY OF IRAC-SELECTED SOURCES FOR THE DEEPER FIELDS.

HzRG	Density (arcmin ⁻²)
PKS1138-262 ($z = 2.156$)	18.1 ± 2.4
MRC0156-252 ($z = 2.016$)	17.8 ± 2.4
MRC0350-279 ($z = 1.900$)	17.5 ± 2.4
MRC1017-220 ($z = 1.768$)	14.3 ± 2.1
MRC2104-242 ($z = 2.491$)	14.0 ± 2.1
MRC2139-292 ($z = 2.550$)	13.7 ± 2.1
MG2308+0336 ($z = 2.457$)	12.1 ± 2.0
USS1425-148 ($z = 2.349$)	12.1 ± 2.0
MRC0324-228 ($z = 1.894$)	11.5 ± 1.9
LBDS53W002 ($z = 2.393$)	10.8 ± 1.9
MRC0406-244 ($z = 2.427$)	10.8 ± 1.9
MRC1324-262 ($z = 2.280$)	8.6 ± 1.7

of the IRAC-selected sources for these 11 cluster candidates. Small gray and large red dots indicate red IRAC-selected sources detected within the 3σ limits of each individual field and to the depth of our survey, respectively. These fields present a very diverse spatial distribution of red sources. Some fields show clumps (e.g., USS1425-148, MRC0350-279) while others show more filamentary structures (e.g., MRC0114-211, 3C470, PKS1138-262).

The fields of MRC0114-211 ($z = 1.41$), 3C470 ($z = 1.65$), MRC2224-273 ($z = 1.68$), MRC0350-279 ($z = 1.90$), MRC2139-292 ($z = 2.55$) and MRC2025-218 ($z = 2.63$) have never been studied for overdensities in the past. They show several clumps of red sources whose association with the targeted radio galaxy still need to be confirmed with spectroscopy. We next briefly discuss each of these cluster candidates in order of increasing redshift.

6.1. MRC0114-211 ($z = 1.41$)

The environment of this radio galaxy had never been studied in the past. This field is the lowest redshift but also the strongest galaxy cluster candidate in the HzRG sample, overdense at a 6σ level compared to SWIRE. Only 0.03% of the cells in our counts-in-cells analysis are found with such density. The distribution of the IRAC-selected red sources shows a clear spatial segregation. The bright red galaxies lie preferentially in two N/S elongated structures with the radio galaxy embedded in the southern one. The northern clump is $2'$ (~ 1 Mpc) north of the radio galaxy. Additional groups of red galaxies are also observed within 1 Mpc of the radio position, suggesting that MRC0114-211 is part of a complex large-scale structure. Furthermore, five red IRAC-selected sources (including the radio galaxy itself) are found in the immediate vicinity (within $15'' \sim 125$ kpc) of the HzRG, corresponding to a density about 9 times higher than average. No other radio galaxy in our sample shows such a dense environment.

6.2. 7C1756+6520 ($z = 1.42$)

Galametz et al. (2009) identified this HzRG as residing in a candidate high-redshift cluster based on BzK photometry. This cluster was recently confirmed in spectroscopy with 21 cluster members (Galametz et al. 2010b). The spatial distribution of the IRAC-selected sources is clumpy, with a main compact clump of bright galaxies $1'$ SE of the radio galaxy. This location coincides with the spectroscopically confirmed sub-group of galaxies in Galametz et al. (2010b) at $z = 1.437$. Seven of the spectroscopically confirmed members were observed and detected both at 3.6 and $4.5\mu\text{m}$. Only one (ID Cl 1756.20 in Galametz et al. 2010b) has an unexpectedly blue IRAC color ($[3.6] - [4.5] = -0.4$). The other six galaxies have $[3.6] - [4.5] > -0.1$.

6.3. 3C470 ($z = 1.65$) and MRC2224-273 ($z = 1.68$)

These fields present very inhomogeneous distributions of IRAC-selected sources. In both cases, the radio galaxies are located (in projection) at the edges of the galaxy overdensities. Spectroscopic follow-up of the structures is required to confirm the association of high-redshift galaxy structures with the radio galaxies.

6.4. MRC0350-279 ($z = 1.90$)

This is the third densest field in our sample. Two very compact clumps of red sources are found within $1'$ and aligned with MRC0350-279 in the direction NW/SE, forming an intriguing symmetrical structure.

6.5. MRC0156-252 ($z = 2.02$)

Galametz et al. (2010a) presented a study of the surroundings of MRC0156-252. In that work, we used a purely near-infrared color criterion to select $z > 2$ galaxies in the field and found that the radio galaxy lies in an overdense region of both early-type and star-forming candidates. The majority of the IRAC-selected sources within $1'$ of MRC0156-252 are found north of the radio galaxy, a result also found for the near-infrared selected cluster candidates in Galametz et al. (2010a).

6.6. *PKS1138-262* ($z = 2.16$)

This radio galaxy (also referred to as the ‘‘Spider Web’’ galaxy) is associated with a well studied high-redshift galaxy protocluster. Several intense programs have studied this field, identifying a diversity of cluster members: Ly α emitters, H α emitters (Pentericci et al. 2000; Kurk et al. 2004a), or candidate cluster members: EROs (Kurk et al. 2004b), Distant Red Galaxies (DRGs; Kodama et al. 2007). To date, only two massive red sources have been spectroscopically confirmed to be associated with PKS1138-262 (Doherty et al. 2010); both are red IRAC-selected sources with $[3.6] - [4.5] > 0.1$. Similar to DRGs selected in this field, the (brightest) IRAC-selected galaxies are preferentially found along a 3’-long E/W filamentary structure (corresponding to the radio axis) in which the radio galaxy is embedded.

6.7. *USS1425-148* ($z = 2.35$)

The environment of this radio galaxy was recently studied using near-infrared observations. Hatch et al. (2011) selected high-redshift galaxies using near-infrared color criteria in the field of six radio galaxies at $z \sim 2.4$. USS1425-148 was the most overdense field of their sample and suspected to contain a high-redshift galaxy cluster at $z > 2$. Fig. 7 suggests that the radio galaxy has several nearby companions. A second clump of sources is found $\sim 1'$ north of USS1425-148.

We note that MRC1324-262 ($z = 2.28$) and MRC0406-244 ($z = 2.427$) were also part of the Hatch et al. (2011) sample and were not found to lie in particularly overdense environments, a result consistent with the present mid-infrared analysis of these fields.

6.8. *4C23.56* ($z = 2.48$)

4C23.56 is also known to lie in an overdense region of galaxies. More than a decade ago, Knopp & Chambers (1997) found an overdensity of red galaxies ($I - K > 4$, Vega) in the immediate surroundings of 4C23.56. A complementary analysis was made by Kajisawa et al. (2006) who found that 4C23.56 was the densest field out of their sample of six radio galaxies at $2.3 < z < 2.6$ in terms of near-infrared cluster galaxy candidates. An excess of candidate H α emitters has also recently been detected in the field by Tanaka et al. (2011), which also reported on the first spectroscopically confirmed companions for 4C23.56, three H α emitters at $z = 2.49$.

6.9. *MRC2139-292* ($z = 2.55$) and *MRC2025-218* ($z = 2.63$)

These fields are our two highest redshift candidates. The field of MRC2139-292 presents a very clear and compact concentration of red galaxies centered on the radio galaxy. Though MRC2025-218 is just above our threshold for identifying rich IRAC environments, we note that Mayo et al. 2012 (in press) find that it resides in a very rich field in the MIPS 24 μ m bandpass, overdense at $\sim 7\sigma$ level compared to control fields.

7. THE MID-INFRARED ENVIRONMENTS OF $Z > 3$ RADIO GALAXIES

The initial sample of HzRGs also comprised 21 galaxies at $z > 3$ that were analyzed in an identical manner to the main sample. Some of these radio galaxies are known to

be within spectroscopically confirmed high-redshift protoclusters (e.g. USS0943-242, TNJ1338-1942, MRC0316-257, TNJ0924-2201; Venemans et al. 2007) though none were recovered by the present mid-infrared analysis. This suggests evolution in the luminosity function of high redshift galaxy clusters. As seen in Fig. 2, the simplest single stellar population models predict relatively constant [4.5] flux densities at $z > 1$ for a wide range of formation redshifts, as well as a brightening of the galaxies as we approach the formation epoch. The fact that we do not recover these known rich (proto-)clusters at $z > 3$ implies that this simple model is incorrect, most likely because the massive ellipticals that comprise the clusters are still in process of forming in a hierarchical manner. Deeper IRAC data from a large sample of clusters and cluster candidates out to $z \sim 3$ should test this hypothesis. We are, in fact, amassing such a data set with the Clusters Around Radio-Loud AGN (CARLA) *Warm Spitzer* snapshot program (Galametz et al. in prep.).

The radio galaxy 4C41.17 ($z = 3.79$) lies in an overdense region of IRAC-selected sources. A compact clump of IRAC-selected sources is observed, slightly offset $1'$ south of the radio galaxy. Ivison et al. (2000) also reported an overdensity of sub-millimeter galaxies in this field, though spectroscopic follow-up has failed to confirm their association with the radio galaxy (Greve et al. 2007). We suspect that there might be a foreground galaxy structure in this field.

8. CONCLUSIONS

We identified overdensities in the fields of powerful HzRGs at $z > 1.2$. We studied the distribution of sources with $[3.6] - [4.5] > -0.1$ using a counts-in-cell analysis, defining a region to be overdense when denser (at the 2σ level) than the SWIRE average, i.e., when 15 or more red IRAC-selected galaxies (with $f_{4.5} \geq 13.4\mu\text{Jy}$) are found in a cell of $1'$ radius. We identified 11 radio galaxies with at least 15 IRAC-selected candidates within $1'$. These 11 radio galaxy fields, representing 23% of our sample of 48 HzRGs, are the most promising galaxy cluster candidates from our analysis. The large fraction of overdense fields clearly indicates that radio galaxies, on average, reside in rich environments. Randomly selecting similarly analyzed samples of 48 control fields from the SWIRE survey, we find such a high fraction of dense fields in only 0.3% of the samples.

Five of these fields have been studied in the past and are known or suspected to contain a (proto-)cluster at high-redshift. Three have been spectroscopically confirmed to be associated with the radio galaxy. This clearly demonstrates the strength of IRAC to select high-redshift galaxy structures. Our relatively shallow data have permitted the recovery of known clusters in very short integration times (120s); past ground-based studies have required hours of optical/near-infrared observations.

We tested for correlations of environment with radio galaxy properties and found no significant trends with either redshift or radio luminosity. We note however that a detailed analysis of evolution of the cluster population with redshift will require an even larger sample of high-redshift clusters as well as a better understanding of the luminosity function for clusters at $z > 1$. No statistically significant trend with radio luminosity was

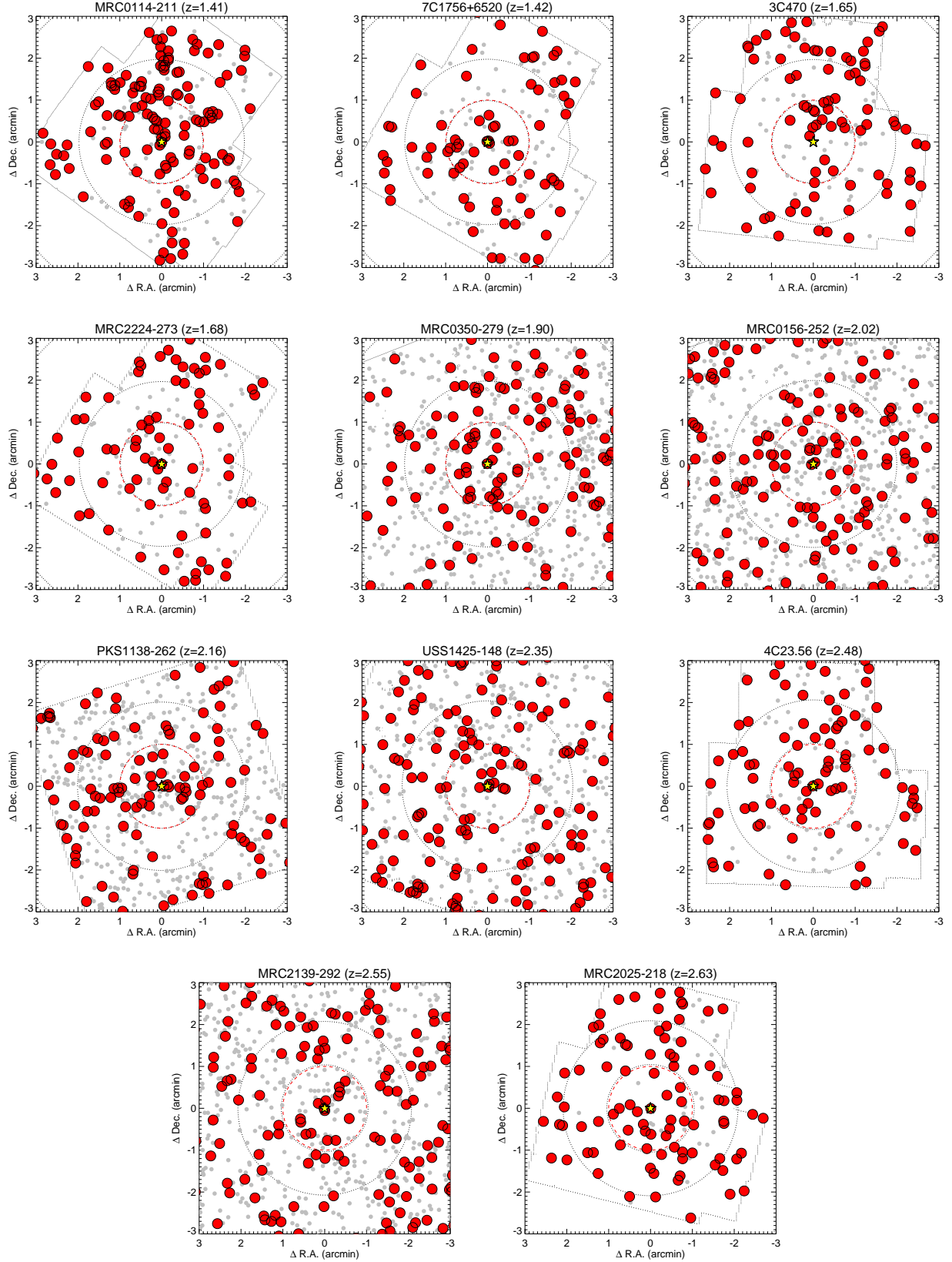


FIG. 7.— Spatial distribution of $[3.6] - [4.5] > -0.1$ galaxies around the radio galaxies with a 2σ excess of IRAC-selected sources compared to SWIRE (i.e., with more than 15 IRAC-selected sources within $1'$). We plot sources down to the 3σ limits of each image (small gray dots) and to the uniform (5σ) limits of our full sample (larger red dots). Contours of the combined IRAC1+2 studied zone are illustrated by the dashed lines. Concentric dotted circles account for distances of 0.5, 1 and 2 Mpc at the redshift of the targeted radio galaxy (yellow star). The red dashed circle shows the cell of $1'$ radius centered on the HzRG and used in the count-in-cell analysis in Section 5. North is up, East is to the left.

observed. Nevertheless, the majority of our cluster candidates are found in the fields of more luminous radio galaxies ($L_{500\text{MHz}} > 10^{28.6} \text{ W Hz}^{-1}$).

This work is based on observations made with the *Spitzer Space Telescope*, which is operated by the Jet Propulsion Laboratory, California Institute of Technology under a contract with NASA. We are very grateful to Mark Brodwin and Peter Eisenhardt for having provided information on the Boötes cluster sample mentioned in this paper and to Conor Mancone for providing his useful EZ Gal Model Generator and valuable help on models. We also thank the anonymous referee for his/her very useful comments.

REFERENCES

- Ashby, M. L. N. et al. 2009, *ApJ*, 701, 428
 Bertin, E. & Arnouts, S. 1996, *A&AS*, 117, 393
 Best, P. N. et al. 2003, *MNRAS*, 343, 1
 Brodwin, M. et al. 2006, *ApJ*, 651, 791
 Bruzual, G. & Charlot, S. 2003, *MNRAS*, 344, 1000
 Cappelluti, N. et al. 2011, *Memorie della Societa Astronomica Italiana Supplementi*, 17, 159
 Daddi, E. et al. 2000, *A&A*, 361, 535
 De Breuck, C. et al. 2004, *A&A*, 424, 1
 —. 2010, *ApJ*, 725, 36
 Demarco, R. et al. 2010, *ApJ*, 711, 1185
 Doherty, M. et al. 2010, *A&A*, 509, 83
 Eisenhardt, P. R. M. et al. 2008, *ApJ*, 684, 905
 —. 2010, *AJ*, 139, 2455
 Falder, J. T. et al. 2010, *MNRAS*, 405, 347
 Fazio, G. G. et al. 2004, *ApJS*, 154, 10
 Galametz, A. et al. 2009, *A&A*, 507, 131
 —. 2010a, *A&A*, 522, A58+
 —. 2010b, *A&A*, 516, A101+
 Gehrels, N. 1986, *ApJ*, 303, 336
 Gladders, M. D. & Yee, H. K. C. 2000, *AJ*, 120, 2148
 Gobat, R. et al. 2011, *A&A*, 526, A133+
 Greve, T. R. et al. 2007, *MNRAS*, 382, 48
 Haas, M. et al. 2009, *ApJ*, 695, 724
 Hatch, N. A. et al. 2011, *MNRAS*, 410, 1537
 Ivison, R. J. et al. 2000, *ApJ*, 542, 27
 John, T. L. 1988, *A&A*, 193, 189
 Kajisawa, M. et al. 2006, *MNRAS*, 371, 577
 Knopp, G. P. & Chambers, K. C. 1997, *ApJS*, 109, 367
 Kodama, T. et al. 2007, *MNRAS*, 377, 1717
 Kurk, J. D. et al. 2004a, *A&A*, 428, 793
 —. 2004b, *A&A*, 428, 817
 Lacy, M. et al. 2005, *ApJS*, 161, 41
 Lonsdale, C. J. et al. 2003, *PASP*, 115, 897
 Macklin, J. T. 1982, *MNRAS*, 199, 1119
 Mancone, C. L. et al. 2010, *ApJ*, 720, 284
 Maraston, C. 2005, *MNRAS*, 362, 799
 Miley, G. & De Breuck, C. 2008, *A&A Rev.*, 15, 67
 Papovich, C. 2008, *ApJ*, 676, 206
 Papovich, C. et al. 2010, *ApJ*, 716, 1503
 Pentericci, L. et al. 2000, *A&A*, 361, L25
 Rettura, A. et al. 2011, *ApJ*, 732, 94
 Rosati, P., Borgani, S., & Norman, C. 2002, *ARA&A*, 40, 539
 Seymour, N. et al. 2007, *ApJS*, 171, 353
 Simpson, C. & Eisenhardt, P. 1999, *PASP*, 111, 691
 Sorba, R. & Sawicki, M. 2010, *ApJ*, 721, 1056
 Stanford, S. A. et al. 2005, *ApJ*, 634, L129
 Stern, D., Holden, B., Stanford, S. A., & Spinrad, H. 2003, *AJ*, 125, 2759
 Stern, D. et al. 2005, *ApJ*, 631, 163
 —. 2007, *ApJ*, 663, 677
 —. 2010, *Journal of Cosmology and Astro-Particle Physics*, 2, 8
 Stevens, J. A. et al. 2003, *Nature*, 425, 264
 Strazzullo, V. et al. 2006, *A&A*, 450, 909
 Tanaka, I. et al. 2011, *PASJ*, 63, 415
 Tanaka, M., Finoguenov, A., & Ueda, Y. 2010, *ApJ*, 716, L152
 van Dokkum, P. G. 2008, *ApJ*, 674, 29
 Venemans, B. P. et al. 2007, *A&A*, 461, 823
 Vikhlinin, A. et al. 2009, *ApJ*, 692, 1033
 Wilson, G. et al. 2009, *ApJ*, 698, 1943
 Yee, H. K. C. et al. 2000, *ApJS*, 129, 475

TABLE 2
THE SHALLOW HzRG SAMPLE (IN REDSHIFT ORDER).

Name	R.A. (J2000)	Dec. (J2000)	z^a	$\log(L_{500\text{MHz}})^b$ (W Hz $^{-1}$)	Density (arcmin $^{-2}$)
3C356.0	17:24:19.0	50:57:40.30	1.079	28.35	2.5 ± 0.9
MRC0037–258	00:39:56.4	–25:34:31.01	1.100	27.72	3.5 ± 1.1
3C368.0	18:05:06.3	11:01:33.00	1.132	28.52	3.2 ± 1.0
6C0058+495	01:01:18.9	49:50:12.29	1.173	27.33	3.8 ± 1.1
3C266	11:45:43.4	49:46:08.24	1.275	28.54	3.8 ± 1.1
MRC0211–256	02:13:30.5	–25:25:21.00	1.300	27.78	2.5 ± 0.9
MRC0114–211	01:16:51.4	–20:52:06.71	1.410	28.66	8.9 ± 1.7
7C1756+6520	17:57:05.4	65:19:53.11	1.4156	27.40	6.4 ± 1.4
7C1751+6809	17:50:49.9	68:08:25.93	1.540	27.46	2.5 ± 0.9
3C470	23:58:35.3	44:04:38.87	1.653	28.79	5.7 ± 1.4
MRC2224–273	22:27:43.3	–27:05:01.71	1.679	27.52	4.8 ± 1.2
6C0132+330	01:35:30.4	33:17:00.82	1.710	27.64	4.1 ± 1.1
3C239	10:11:45.4	46:28:19.75	1.781	29.00	2.2 ± 0.8
3C294.0	14:06:44.0	34:11:25.00	1.786	28.96	2.9 ± 1.0
7C1805+6332	18:05:56.9	63:33:13.14	1.840	27.78	4.5 ± 1.2
6CE0820+3642	08:23:48.1	36:32:46.42	1.860	28.28	1.6 ± 0.7
6CE0905+3955	09:08:16.9	39:43:26.00	1.883	28.17	3.5 ± 1.0
6CE0901+3551	09:04:32.4	35:39:03.23	1.910	28.19	3.2 ± 1.0
MRC0152–209	01:54:55.8	–20:40:26.30	1.920	28.20	3.8 ± 1.1
MRC2048–272	20:51:03.6	–27:03:02.53	2.060	28.72	4.5 ± 1.2
5C7.269	08:28:38.8	25:28:27.10	2.218	27.82	2.2 ± 0.8
4C40.36	18:10:55.7	40:45:24.01	2.265	28.79	2.9 ± 1.0
TXS0211–122	02:14:17.4	–11:58:46.00	2.340	28.48	4.1 ± 1.1
USS1707+105	17:10:06.5	10:31:06.00	2.349	28.63	1.6 ± 0.7
USS1410–001	14:13:15.1	–00:22:59.70	2.363	28.41	1.3 ± 0.6
6C0930+389	09:33:06.9	38:41:50.14	2.395	28.41	2.2 ± 0.8
3C257	11:23:09.2	05:30:19.47	2.474	29.16	3.2 ± 1.0
4C23.56	21:07:14.8	23:31:45.00	2.483	28.93	6.4 ± 1.4
USS1558–003	16:01:17.3	–00:28:48.00	2.527	28.82	3.8 ± 1.1
WNJ1115+5016	11:15:06.9	50:16:23.92	2.540	27.82	1.3 ± 0.6
USS0828+193	08:30:53.4	19:13:16.00	2.572	28.44	3.2 ± 1.0
PKS0529–549	05:30:25.2	–54:54:22.00	2.575	29.16	2.2 ± 0.8
MRC2025–218	20:27:59.5	–21:40:56.90	2.630	28.74	5.7 ± 1.3
USS2202+128	22:05:14.1	13:05:33.50	2.706	28.54	2.2 ± 0.8
MG1019+0534	10:19:33.4	05:34:34.80	2.765	28.57	3.2 ± 1.0
4C24.28	13:48:14.8	24:15:52.00	2.879	29.05	2.9 ± 1.0
4C28.58	23:51:59.2	29:10:28.99	2.891	28.91	3.8 ± 1.1
USS0943–242	09:45:32.7	–24:28:49.65	2.923	28.62	2.9 ± 1.0
WNJ0747+3654	07:47:29.4	36:54:38.09	2.992	28.14	2.5 ± 0.9
B3J2330+3927	23:30:24.9	39:27:12.02	3.086	28.33	1.3 ± 0.6
WNJ0617+5012	06:17:39.4	50:12:55.40	3.153	28.02	3.9 ± 1.1
MRC0251–273	02:53:16.7	–27:09:13.03	3.160	28.54	2.5 ± 0.9
WNJ1123+3141	11:23:55.9	31:41:26.14	3.217	28.51	2.9 ± 1.0
6C1232+39	12:35:04.8	39:25:38.91	3.220	28.93	2.5 ± 0.9
TNJ0205+2242	02:05:10.7	22:42:50.40	3.506	28.46	1.6 ± 0.7
TNJ0121+1320	01:21:42.7	13:20:58.00	3.516	28.49	3.2 ± 1.0
TXJ1908+7220	19:08:23.7	72:20:11.82	3.53	29.12	5.4 ± 1.3
USS1243+036	12:45:38.4	03:23:20.70	3.570	29.23	4.1 ± 1.1
WNJ1911+6342	19:11:49.6	63:42:09.60	3.590	28.14	1.9 ± 0.8
MG2144+1928	21:44:07.5	19:29:14.60	3.592	29.08	3.5 ± 1.1
6C0032+412	00:34:53.1	41:31:31.50	3.670	28.75	1.9 ± 0.8
4C60.07	05:12:54.8	60:30:52.01	3.788	29.20	4.1 ± 1.1
TNJ2007–1316	20:07:53.3	–13:16:43.62	3.840	29.13	3.2 ± 1.0
8C1435+635	14:36:37.1	63:19:14.00	4.250	29.40	2.5 ± 0.9
TNJ0924–2201	09:24:19.9	–22:01:41.00	5.195	29.51	1.0 ± 0.6

^a Our analysis focusses on fields around HzRGs with $1.2 < z < 3$. The other fields are used as control fields.

^b Radio luminosities from De Breuck et al. (2010).

TABLE 3
THE DEEPER SPITZER SAMPLE (IN REDSHIFT ORDER).

Name	R.A. (J2000)	Dec. (J2000)	z ^a	$\log(L_{500\text{MHz}})$ ^a (W Hz ⁻¹)	IRAC Exp. Time (s)	PID	Density (arcmin ⁻²)
LBDS53W091	17:22:32.7	50:06:01.94	1.552	27.04	900	65	3.8 ± 1.1
MRC1017-220	10:19:49.0	-22:19:58.03	1.768	27.94	1600	60112	4.5 ± 1.2
MRC0324-228	03:27:04.4	-22:39:42.60	1.894	28.49	1600	60112	2.9 ± 1.0
MRC0350-279	03:52:51.6	-27:49:22.61	1.900	28.25	1600	60112	8.0 ± 1.6
MRC0156-252	01:58:33.6	-24:59:31.10	2.016	28.46	1600	60112	5.1 ± 1.3
PKS1138-262	11:40:48.6	-26:29:08.50	2.156	29.07	3000	17	8.3 ± 1.6
MRC1324-262	13:26:50.82	-26:30:51.10	2.280	28.45	1600	60112	1.9 ± 0.8
USS1425-148	14:28:52.50	-15:01:37.50	2.349	28.66	1600	60112	5.4 ± 1.3
LBDS53W002	17:14:14.7	50:15:29.70	2.393	27.78	3300	211	4.1 ± 1.1
MRC0406-244	04:08:51.5	-24:18:16.39	2.427	29.03	1600	60112	3.8 ± 1.1
MG2308+0336	23:08:28.05	03:36:20.70	2.457	28.51	1600	60112	4.5 ± 1.2
MRC2104-242	21:06:58.1	-24:05:11.00	2.491	28.84	1600	60112	4.1 ± 1.1
MRC2139-292	21:42:16.7	-28:58:40.00	2.550	28.73	1600	60112	4.8 ± 1.2
MRC0316-257	03:18:12.0	-25:35:11.00	3.130	28.95	46000	3482	3.8 ± 1.1
B20902+34	09:05:30.1	34:07:56.89	3.395	28.78	1200	64	3.2 ± 1.0
4C41.17	06:50:52.1	41:30:31.00	3.792	29.18	5000	79	6.7 ± 1.5
TNJ1338-1942	13:38:26.0	-19:42:31.00	4.110	28.71	5000	17	3.8 ± 1.1
6C0140+326	01:43:43.8	32:53:49.31	4.413	28.73	5000	79	4.5 ± 1.2

^a Our analysis focusses on fields around HzRGs with $1.2 < z < 3$. The other fields are used as control fields.

^b Radio luminosities from De Breuck et al. (2010).